symmetry

MDPI

Article

Influence of Symmetry from Crystal Structure and Chemical Environments of Magnetic Ions on the Fully Compensated Ferrimagnetism of Full Heusler Cr_2YZ and Mn_2YZ Alloys

Zhigang Wu [1], Yajiu Zhang [1,*], Zhuhong Liu [2] and Xingqiao Ma [2]

[1] School of Civil Engineering, Guangzhou University, Guangzhou 510006, China; zgwu@gzhu.edu.cn
[2] Department of Physics, University of Science and Technology Beijing, Beijing 100083, China; zhliu@ustb.edu.cn (Z.L.); xqma@sas.ustb.edu.cn (X.M.)
* Correspondence: yjzh@gzhu.edu.cn

Abstract: Fully compensated ferrimagnets do not create any magnetic stray field and allow for a completely polarized current of charges. As a result, these alloys show promising prospects for applications as spintronic devices. In this paper, we investigated the phase stability, the site preference, the tetragonal distortion and the influence of symmetry from the crystal structure and chemical environments of magnetic ions on the magnetic properties of Cr_2YZ and Mn_2YZ (Y = void, Ni, Cu, and Zn; Z = Ga, Ge, and As) full Heusler alloys by first-principles calculations. We found that the selected Cr_2-based alloys, except for Cr_2NiGa and Cr_2NiGe, prefer to crystallize in the centrosymmetric $L2_1$-type structure, while the selected Mn_2-based alloys, except for Mn_2CuAs, Mn_2ZnGe and Mn_2ZnAs, tend to crystallize in the non-centrosymmetric XA-type structure. Due to the symmetry, the antiferromagnetism of the selected $L2_1$-type alloys is very stable, and no spin-polarized density of states could be generated. In contrast, the magnetic moment of the selected XA-type alloys depends heavily on the number of valence electrons and tetragonal distortion, and spin-polarized density of states is generated. Therefore, the selected alloys with $L2_1$-type structures and their tetragonal-distorted structure are potential candidates for conventional antiferromagnets, while those with XA-type structure and their tetragonal-distorted structure are promising candidates for (fully) compensated ferrimagnets.

Keywords: fully compensated ferrimagnets; Heusler alloys; first-principles calculations; symmetry

Citation: Wu, Z.; Zhang, Y.; Liu, Z.; Ma, X. Influence of Symmetry from Crystal Structure and Chemical Environments of Magnetic Ions on the Fully Compensated Ferrimagnetism of Full Heusler Cr_2YZ and Mn_2YZ Alloys. *Symmetry* **2022**, *14*, 988. https://doi.org/10.3390/sym14050988

Academic Editors: Xiaolei Wang, Xueyun Wang and Chao Shen

Received: 7 April 2022
Accepted: 9 May 2022
Published: 12 May 2022

1. Introduction

Spintronic devices based on antiferromagnets (AFMs) have attracted great interest in recent years [1,2]. The most important characteristic of AFM materials is net-zero magnetic moment; thus, they do not carry any macroscopic magnetic field [3]. The spintronic devices based on AFM materials are not easily interfered with by external magnetic fields and do not generate stray fields to disturb adjacent devices [4]. Recent studies also show that AFM materials display ultrafast dynamics and generate large magneto-transport effects [5]. There are two different kinds of AFMs. One is the conventional AFM, such as metals Mn and Cr, which has a zero net spin magnetic moment and zero spin polarization (Figure 1a). The other is called half-metallic AFM (HMAFM), which was proposed by Van Leuken and Groot in the 1990s [6]. HMAFM is a special kind of ferrimagnet, which has reduced symmetry, half-metallic band structure and zero net magnetic moment at the same time. Therefore, a more precise term for HMAFM is half-metallic fully compensated ferrimagnets (HMFCFs), proposed by later researchers [7–10]. The following discussion will use the term HMFCF to represent this type of material. As shown in Figure 1b, the electronic structure of HMFCFs is fully spin polarized near the Fermi level. HMFCFs have the following properties: (1) create no magnetic stray field, (2) contribute a 100% spin-polarized charge, and (3) the magnetic susceptibility is zero.

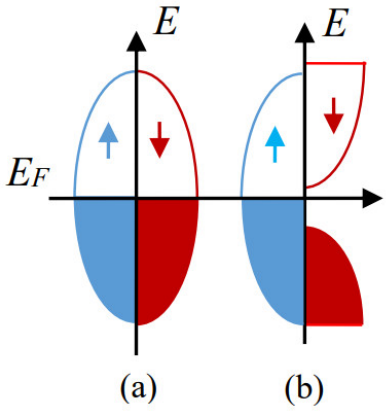

Figure 1. Schematic diagram of density of states for conventional AFM (**a**) and (**b**) HMFCF. E_F is the Fermi Energy.

Based on these features, HMFCFs could be even more useful than half-metallic ferromagnets (HMFs) and conventional AFM. The high spin polarization provides the possibility of reaching high magnetoresistance and low magnetic damping, while the zero net magnetic moment can lead to high storage density due to the absence of a stray field. In contrast to a conventional AFM, compensated ferrimagnets have reduced symmetry and allow for easier magnetic reading and writing. These unique properties make compensated ferrimagnets promising for fast, energy-efficient spintronic devices, such as spin-polarized scanning tunneling microscopy (SP-STM) tips, anchor layer in a spin valve and spin-orbit torque [9,11]. Experimental evidence of HMFCFs was recently observed in Heusler-type $Mn_2Ru_{0.5}Ga$ [12]. To date, many alloys (e.g., Ti_2YZ (Y = V, Cr, Mn; Z = Al, Ga, In, Ge, P, As, Sb) [13–18], Cr_2MnZ [19,20], Co-doped Mn_2VZ [21], Cr_2YZ [22], Cr_2CoGa [23], Mn_2Ru_xGa [24], Mn_2Z (Z = Si, Ge, Sn) [25–27], CrVTiAl [28,29], FeMnGa [30], and Sr_2OsMoO_6 [31]) have been predicted to be HMFCFs by electronic structure calculations. Most of them are Heusler alloys, which are a kind of intermetallic compound and an important material family in condensed matter physics and material science [32,33].

In Heusler alloys, there are several key points for the formation of HMFCFs. One of them is the number of valence electrons (N_V) per unit cell of the alloys. The total spin magnetic moment (M_t) of a half-metal is quantized, and the relationship between M_t and N_V follows the famous Slater–Pauling (SP) rule [34]. There are three modes of SP rule in Heusler alloys, which are $M_t = N_V - 18$, $M_t = N_V - 24$ and $M_t = N_V - 28$ [35,36]. Therefore, only Heusler alloys with N_V = 18, 24, or 28 will get a zero net magnetic moment. Generally, the number of magnetic ions in the alloys is also a key point to obtain HMFCF. An even number of magnetic ions may lead to conventional AFM because of the inversion symmetry of the magnetic structure. Three or more magnetic ions are usually necessary to break the inversion symmetry to get the FCF property [29]. However, the recently proposed $C1_b$-type HMFCF Mn_2Z (Z = Si, Ge and Sn) alloys do not meet the condition, since they have only two magnetic ions per unit cell but exhibit a typical FCF state [16,27].

Mn_2YZ (Y = transition metals; Z = main group elements) full Heusler alloys, due to their diverse magnetic and unique electronic properties, are promising candidates for HMFs [37], HMFCFs [12,21], thermoelectrics [38], magnetic skymions [39], exchange bias, [40,41] and spin gapless semiconductors [42]. Most of them have higher Curie temperatures (T_C) than room temperature, which makes them beneficial for practical applications. Cr_2YZ (Y = transition metal; Z = main group elements) full Heusler alloys have been recently proposed, with the same crystal structure as Mn_2YZ, to show similar potential applications in spintronics [19,20,22,23]. Antiparallel aligned magnetic moments, which are formed between Mn (Cr) atoms of different sublattices, are important for the formation of compensated ferrimagnetic state. Mn_2YZ and Cr_2YZ alloys have two inequivalent structure configurations, the non-centrosymmetric XA-type structure (F-43m, space group no. 216) and the centrosymmetric $L2_1$-type structure (Fm-3m, space group no. 225). The

difference in the symmetry of the crystal structure might have a significant effect on the magnetic properties and density of states distribution, which, in turn, affects the formation of HMFCF.

The current research focuses mainly on alloys with a low number of valence electrons (N_V) of Y, such as Y = Ti, V, Cr, Mn, Fe, and Co [36,43]. Few studies focus on alloys with high N_V of Y, such as Y = Cu and Zn. Cu and Zn tend not to contribute local magnetic moments in Heusler alloys. Ferromagnetic Ni atoms also hardly contribute significant magnetic moments in Heusler alloys. Therefore, it is advantageous to study the influence of crystal structure symmetry on the magnetic and electronic density of states distribution in Mn_2YZ and Cr_2YZ (Y = Ni, Cu and Zn; Z = main group element) alloys, since Ni, Cu, an Zn do not contribute to the magnetic properties at all, and the number of magnetic ions is even.

Mn_2YZ systems with a tetragonal structure or a spontaneous structural transition from cubic phase to tetragonal phase have important properties for applications, such as the perpendicular magnetic anisotropy (PMA) for spin-transfer torque magnetic random-access memory (STT MRAM) [44], and the ferromagnetic shape memory alloys (FSMAs) [45]. As alloys similar to Mn_2YZ, the tetragonal distortion of Cr_2YZ has been less studied. The tetragonal phase (I4/mmm, space group no. 139) distorted from the $L2_1$-type cubic phase remains centrosymmetric, while the tetragonal (I-4m2, space group no. 119) distorted from the XA-type cubic phase is noncentrosymmetric. The difference in the symmetry of these two tetragonal structures will also lead to the difference in the magnetic and electronic properties, which require further study.

In this paper, we investigated the phase stability, the site preference, tetragonal distortion, and the influence of symmetry from crystal structure and chemical environments of magnetic ions on the electronic and magnetic properties of Cr_2YZ and Mn_2YZ (Y = void, Ni, Cu, and Zn; Z = Ga, Ge, and As) full Heusler alloys by first-principles calculations. Void means that no atoms were selected for Y, such as Cr_2Z and Mn_2Z. It should be noted that the $C1_b$-type and C1-type structures have the same symmetry as the $L2_1$-type and XA-type structures, respectively. Void can be regarded as a different atom from Mn or Cr, so Mn_2 (void) Z and Cr_2 (void) Z can be regarded as special full-Heusler alloys. All these alloys, except for Cr_2NiZ and Mn_2NiZ, have two magnetic ions per unit cell. Our results indicate that the selected alloys with centrosymmetric $L2_1$ types and their tetragonally distorted structure are conventional AFMs, while those with non-centrosymmetric XA types and their tetragonally distorted structure are candidates for (fully) compensated ferrimagnets.

2. Calculation Method

The first-principles calculations based on density of functional theory (DFT) were performed with Vienna ab-initio simulation package (VASP) [46]. The generalized-gradient approximation (GGA) in the Perdew–Burke–Ernzerhof (PBE) was employed to deal with the electronic exchange and correlation. Previous calculation indicates that the results obtained by GGA are in good agreement with the experiment results in 3d Heusler alloys [42]. The projector-augmented wave (PAW) was selected to describe the electron–ion interaction [47,48]. To achieve good convergence, the cut-off energy was set to 500 eV for all of the calculations, and 15 × 15 × 15 k-points were used for reciprocal spatial integration. The convergence criteria for the calculation were chosen as the total energy tolerance within 10^{-6} eV and the atomic force tolerance within 0.01 eV/Å. According to Mavropoulos et al. [49], the effect of spin–orbit coupling on the band gap of Heusler alloys is negligible for 3d transition elements. As such, the spin–orbit coupling was not considered in this work. A full-potential method (FP-LAPW implemented in the WIEN2k code [50], GGA + PBE, and appropriate parameters, such as $R_{MT} \times K_{max}$ = 9, 10,000 k-points in the Brillouin zone and the cut off energy of −6 Ry, have been chosen) was also used to repeat some calculations to confirm the validity of the results obtained by pseudopotential method of VASP.

3. Results and Discussion

We first took Mn_2Si as an example to start the discussion. The $C1_b$-type Mn_2Si was proposed as a potential candidate for FCF with spin gapless semiconducting (SGS) properties [16]. The crystal structure of $C1_b$-type Mn_2Si has three *fcc* sublattices, with Mn (A), Mn (B), and Si occupying Wyckoff coordinates A (0, 0, 0), B (0.25, 0.25, 0.25) and D (0.75, 0.75, 0.75), respectively. Figure 2a,b show the band structures of $C1_b$-type Mn_2Si, calculated by the pseudopotential method and the full-potential method, respectively. Both the calculation methods give the same band structure. This result indicates the validity of the pseudopotential method for 3*d* transition Heusler alloys. Figure 2c displays the corresponding density of states (DOS) of $C1_b$-type Mn_2Si. The DOS of the spin-down channel clearly exhibits a band gap near the Fermi energy (E_F), while the DOS of the spin-up channel shows a vanishingly small gap. As shown by Wang et al. [51], the DOS indicates a typical characteristic of a spin gapless semiconductor (SGS) and, thus, allows for tunable spin transport. Figure 2d gives the total and atom-resolved magnetic moments as a function of the lattice constant. The zero net total magnetic moment indicates the FCF property. Similar behavior was also observed in many other HMFCFs.

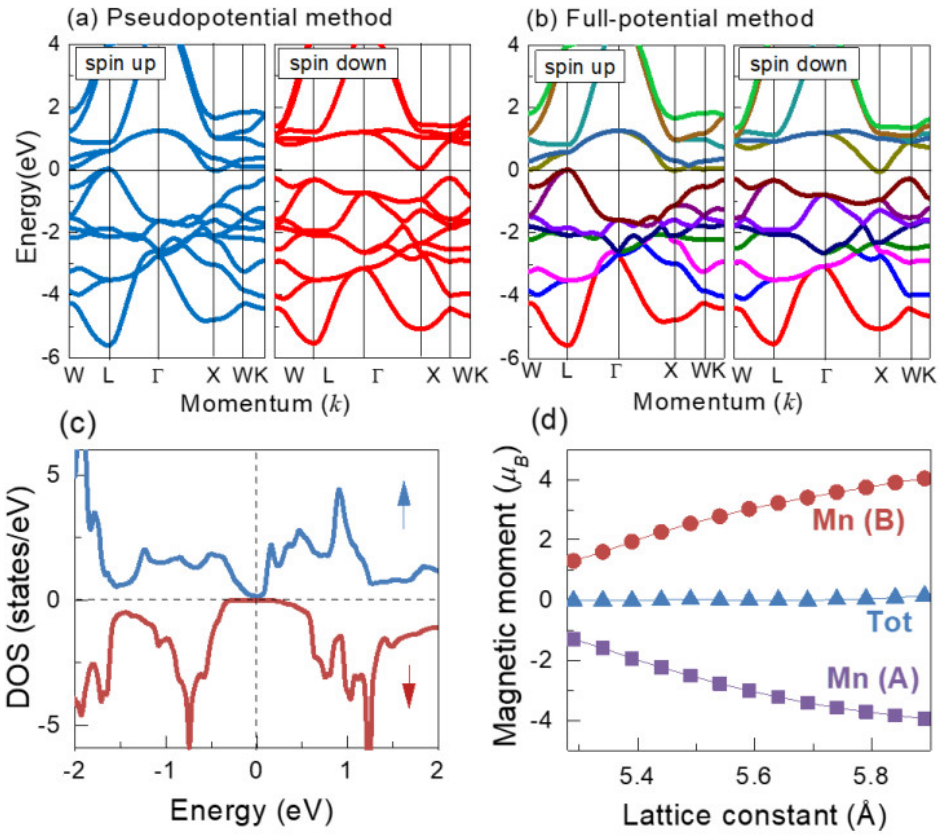

Figure 2. Band structure of $C1_b$-type Mn_2Si calculated by pseudopotential method (**a**) and by full-potential method (**b**) at the equilibrium state, (**c**) spin-polarized DOS, (**d**) magnetic moments as functions of the lattice parameter for Mn (A), Mn (B) and Mn_2Si.

HMFCF behaviors have also been identified in many Heusler alloys, such as $C1_b$-type CrMnSb [52], $L2_1$-type (or DO_3-type) Mn_3Ga [53] and XA-type Cr_2ZnZ (Z = Si, Ge, Sn) [54]. These materials represent three typical crystal structures of Heusler alloys for HMFCF. Although they have different numbers of magnetic ions, a common characteristic of these alloys is that the relationship between their N_V (which is 18, 24 and 28 for CrMnSb, Mn_3Ga, and Cr_2ZnZ, respectively) and M_t (which is zero for all three alloys) follows the Slater–Pauling rule. The $M_t = 0$ and $N_V = 18$ of Mn_2Si, just like other HMFCFs that follow the Slater–Pauling rule in the form of $M_t = N_V - 18$. It should be noted that Heusler alloys,

which are not HMFCFs but have zero net magnetic moments, also exit, such as Fe_2VAl and CoFeTiGa (Al) [55,56]. Since these alloys are not our focus, they will not be discussed in detail. In the following part, we studied the influence of the symmetry of crystal structure and chemical environments of magnetic ions on the electronic and magnetic properties of the Mn_2Si alloy.

We firstly analyzed the electronic properties of three cases: $C1_b$-type Mn_2Si, C1-type Mn_2Si, and ZnS-type Mn_2 in a Heusler matrix. The Heusler matrix has four *fcc* sublattices, which are represented by four Wyckoff coordinates, A (0, 0, 0), B (0.25, 0.25, 0.25), C (0.5, 0.5, 0.5), and D (0.75, 0.75, 0.75). It should be noted that the $C1_b$-type Mn_2Si is energy stable according to the previous work, and the other two cases were employed for comparative discussion only. Figure 3 and Table 1 provide the information of crystal structures for the above three cases. The $C1_b$-type configuration is the so-called half-Heusler, which has a non-centrosymmetric crystal structure (*F*-43*m*, space group no. 216). In the unit cell of this crystal structure, one Mn occupies site A (denoted as Mn (A)), the other Mn occupies site B (denoted as Mn (B)), no atom (void) occupies site C, and Si occupies site D. It can be seen that these two Mn atoms possess different chemical environments. There are four Mn (B) atoms and four Si atoms as the nearest neighbors of Mn (A). However, Mn (B) has only four Mn (A) atoms as the nearest neighbors. In the situation of C1-type Mn_2Si, which has a centrosymmetric crystal structure (F*m*-3*m*, space group no. 225), two Mn atoms occupy site A and site C (denoted as Mn (A) and Mn (C), respectively). In this structure, Mn (A) and Mn (C) have the same chemical environments. Each Mn has only four Si atoms as its nearest neighbors. Figure 3c shows that the Mn (A) and Mn (B) of Mn_2Si form a ZnS (or diamond) structure as Si is removed from the $C1_b$-type Mn_2Si matrix. Due to the removing of Si atoms, the ZnS-type Mn_2 matrix becomes a centrosymmetric structure (*FD*-3*m*, space group no. 227). In this case, these two Mn atoms have the same neighbor conditions: each Mn has four other Mn atoms as its nearest neighbors. The difference of ZnS-type Mn_2 from C1-type Mn_2Si is that the nearest neighbor for each Mn atom comprises four Mn atoms instead of four Si atoms. Next, we analyzed the electronic structures of these three types of configurations.

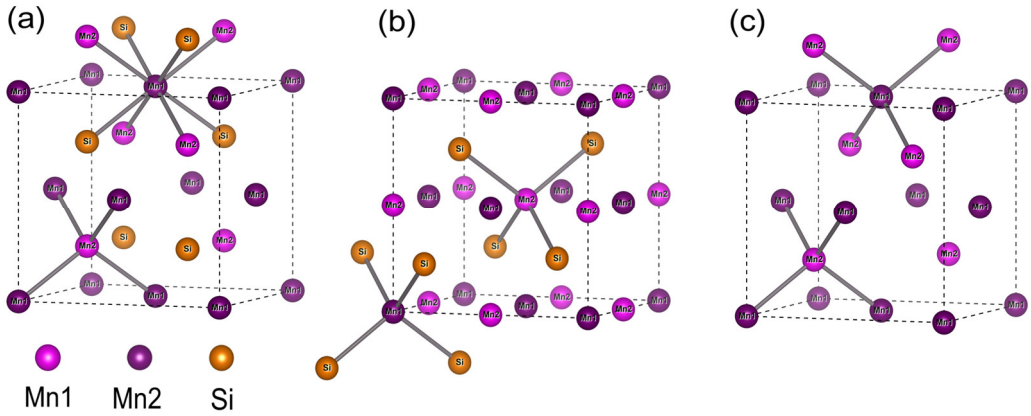

Figure 3. Schematic representation of $C1_b$-Mn_2Si (**a**), ZnS-Mn_2 (**b**), and C1-Mn_2Si (**c**) in a Heusler matrix. Here, C site is vacant for $C1_b$-Mn_2Si, C and D sites are vacant for ZnS-Mn_2, and B site is vacant for C1-Mn_2Si. Mn1 and Mn2 in C1-Mn_2Si are denoted at Mn (A) and Mn (C), while those in $C1_b$-Mn_2Si and ZnS-Mn_2 are denoted as Mn (A) and Mn (B) since they occupy the different Wyckoff coordinates.

Table 1. The crystal structure and corresponding chemical environments of first nearest neighbors (Fnn) of each Mn atom of studied compounds.

Compd.	Structure	Space Group	Group No.	Fnn of Mn_1	Fnn of Mn_2
Mn_2Si	$C1_b$	F-43m	216	4Mn2, 4Si	4Mn1
Mn_2Si	C1	Fm-3m	225	4Si	4Si
Mn_2	ZnS	FD-3m	227	4Mn2	4Mn1

In a conventional AFM, the number of states (NOS) below the Fermi level in the spin-up channel is the same as that in the spin-down channel. The NOS can be obtained by integrating the DOS. As shown in Figure 4, both spin-up and spin-down channels have nine valance electrons per unit, which are from $1 \times s$ of Si, $3 \times p$ of Si, $2 \times e_g$ of Mn and $3 \times t_{2g}$ of Mn, below the Fermi level. It should be noted that the configurations of NOS for $C1_b$-type Mn_2Si are different in the two spin channels. There is a platform that exists in the spin-down channel. Within the range of this platform, the NOS is constant. For C1-type Mn_2Si, the configurations of NOS for the two spin channels are completely identical, indicating a normal AFM state. In addition, the spin-up and spin-down channels of ZnS-type Mn_2 also have the same number of NOS below the Fermi level, which was not shown in the figure.

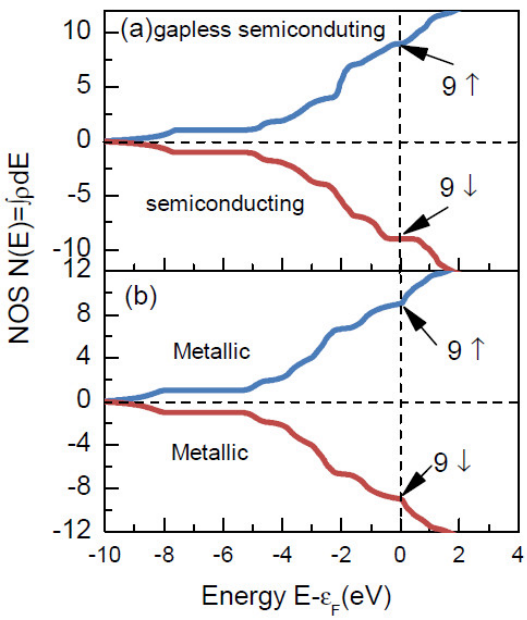

Figure 4. Integrated DOS of $C1_b$-Mn_2Si (**a**) and C1-Mn_2Si (**b**).

Figure 5 shows the distribution of the partial density of states (PDOS) for the two Mn atoms and the net spin state of the unit cell as a function of energy. The PDOS of $C1_b$-type Mn_2Si (Figure 5a) exhibits two important characteristics. The first one is the spin-polarized PDOS of Mn (A) and Mn (B). The PDOS in the spin-down channel has an energy gap with a considerable size near the Fermi level, and that in the spin-up channel has a valley corresponding to a small energy gap. The second characteristic is that the distributions of PDOS in Mn (A) and Mn (B) are not identical, which results in a net spin distribution as a function of energy, as shown in the lower panel. This result corresponds to the different chemical environments between Mn (A) and Mn(B). For C1-type Mn_2Si (Figure 5b) and ZnS-Mn_2 (Figure 5c), the DOS of Mn (A) atoms are identical to that of Mn (B) atoms. The only difference is that the net spin of each Mn atom is opposite. The net spin of the total DOS is zero in all energy ranges, which indicates that no polarization can be obtained at any energy range.

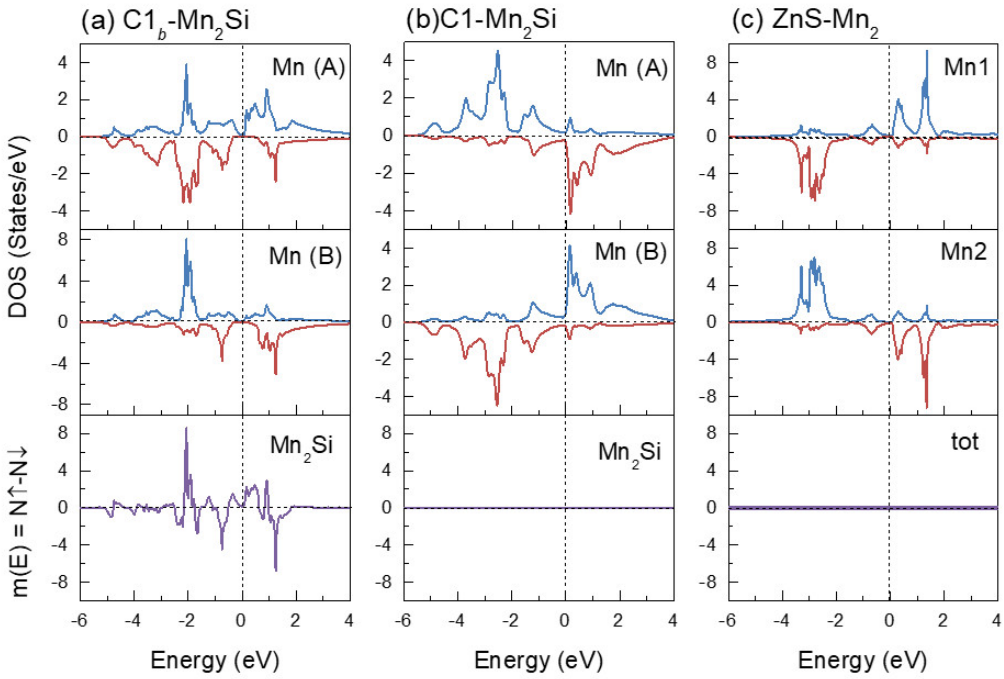

Figure 5. Atomic-resolved PDOS and the net DOS of total as a function of energy for C1$_b$-Mn$_2$Si (**a**), C1-Mn$_2$Si (**b**), and ZnS-Mn$_2$ (**c**).

As such, the distribution of the spin is strongly dependent on the symmetry of the crystal structure and the chemical environments of each Mn atom. As discussed above, C1$_b$-type Mn$_2$Si has a non-centrosymmetric crystal structure, and the first nearest neighbor environments of the Mn ions differ from each other. Mn (A) and Mn (C) in C1-Mn$_2$Si have the same chemical environments. The situation is similar for ZnS-Mn$_2$. The result is a similar situation where there is no spin polarization at all. In C1$_b$-Mn$_2$Si, the differing chemical environments of each Mn atom result in fully spin-polarized DOS, although the Si atoms are nonmagnetic. These results indicate that the asymmetrical chemical environments broke the rotational symmetry of the spins, which led to an asymmetrical distribution of spin-up and spin-down states as a function of energy. As such, broken spin rotational symmetry can be regarded as a key point to obtain HMFCF, which comprises a system without a spontaneous magnetization but with 100% spin polarization in the charge carriers at E_F. Only C1$_b$-type Mn$_2$Si has the asymmetric configurations of DOS for the two spin channels.

In order to further reveal the influence of symmetry from the crystal structure on magnetic properties, we investigated the phase stability, the site preference, the tetragonal distortion, and the magnetic and electronic properties of full-Heusler Cr$_2YZ$ and Mn$_2YZ$ (Y = Ni, Cu, and Zn; Z = Ga, Ge, and As) alloys. There are two non-equivalent crystal lattices for full-Heusler alloys. When the Y atoms occupy site C of the Heusler matrix, as shown in Figure 3a, a non-centrosymmetric XA-type crystal structure, which has the same symmetry as C1$_b$-type Mn$_2$Si, will be formed. When Y atoms occupy site B of the Heusler matrix, as shown in Figure 3b, a centrosymmetric $L2_1$-type structure, which has the same symmetry as C1-type Mn$_2$Si, will be formed.

In Heusler alloys, the atomic site preference is related to the N_V of the 3d transition metallic elements. Generally, elements with lower N_V tend to occupy site B of the Heusler matrix, while those with higher N_V occupy site A and site C of the Heusler matrix. This site preference rule has been proved to be valid in many Heusler alloys [57–61]. According to such a rule, the selected Cr$_2$-based and Mn$_2$-based alloys in the present work should all be crystallized into the XA-type crystal structure.

To determine the theoretical lattice parameters and the site preference, we performed structural optimization calculations on the selected Cr$_2YZ$ and Mn$_2YZ$ (Y = void, Ni, Cu,

and Zn; Z = Ga, Ge, and As) alloys, for both $L2_1$-type and XA-type configurations. The free energy difference (ΔE) between XA-type and $L2_1$-type structures, which is $\Delta E = E$ (XA) $-$ E ($L2_1$), was selected as the y-axis, as shown in Figure 6, which shows the N_V-dependent ΔE of the selected alloys. The fact that $\Delta E < 0$ suggests that XA-type configuration is more energy stable than $L2_1$-type configuration, whereas $L2_1$ is more stable. The calculation results show that the selected Cr_2YZ alloys, except for Cr_2NiGa and Cr_2NiGe, prefer to crystallize into the centrosymmetric $L2_1$-type structure, while the selected Mn_2YZ alloys, except for Mn_2CuAs, Mn_2ZnGe, and Mn_2ZnAs, tend to crystallize into a non-centrosymmetric XA-type structure. These results of the atomic occupations of the selected alloys apparently deviate from the conventional site preference rule of full-Heusler alloys. This result indicates the complexity of the phase stability of Heusler alloys. Similar situations also occurred in Ti_2-based and V_2-based full-Heusler alloys [62,63]. It should be noted that for each transition metal, such as Cr_2CuZ, as Z progresses from Ga through Ge to As, the ΔE increases by about the same amount, except for the Mn2(Void)Z family, where there is a decrease. There might be some particular reason for this.

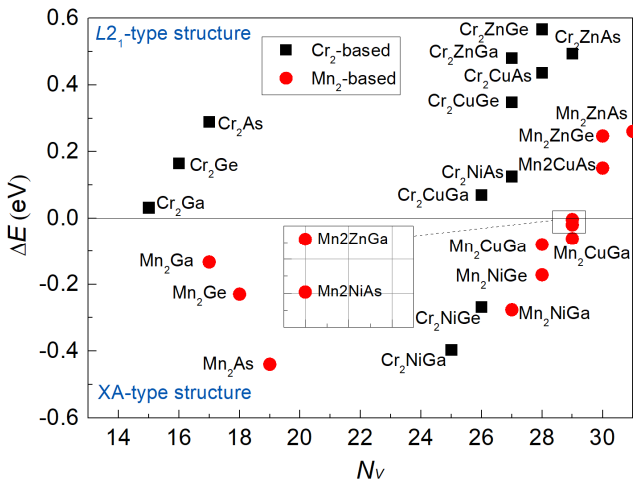

Figure 6. Free energy difference (ΔE) between XA-type and $L2_1$-type structures, $\Delta E = E$ (XA) $-$ E ($L2_1$), for Cr_2YZ and Mn_2YZ (Y = void, Ni, Cu, and Zn; Z = Ga, Ge, and As). The case of $\Delta E < 0$ suggests the XA-type structure of the alloy is more energy stable, while $\Delta E > 0$ indicates a $L2_1$-type structure of the alloy.

To confirm the thermal stability of the selected alloys, the formation energy (E_F) is determined by the formula of $E_F = E_{(Cr\ or\ Mn)\ 2YZ} - (2E_{(Cr\ or\ Mn)} + E_Y + E_Z)$ [64–66], where E_{Cr2YZ} and E_{Mn2YZ} are the total free energy of the selected alloys per unit cell at their equilibrium states, $E_{(Cr\ or\ Mn)}$, E_Y, and E_Z are the free energy per atom of pure metals (Cr or Mn), Y and Z, respectively. Figure 7 gives the values of the E_F of the selected alloys for the energy-stable state that was determined in Figure 6. The negative value of E_F indicates most of the selected alloys can be obtained in experiments. The positive values of E_F for Cr_2Ga, Cr_2Ge, Mn_2Ga, Cr_2CuGe, Cr_2CuAs, Cr_2ZnAs, and Mn_2ZnAs indicate that the $L2_1$-type or XA-type cubic phase of these alloys are energetically unstable in experiments. For example, bulk Mn_2Ga crystallizes into Al_3Ti structure type, which belongs to the space group $I4/mmm$ [24]. However, $C1_b$-Mn_2Ga films were recently successfully grown on V (001) epitaxial films [12], which indicates that the cubic phase of the above alloys also has a possibility to be realized in experiments using advanced preparation methods (e.g., molecular beam epitaxy technology).

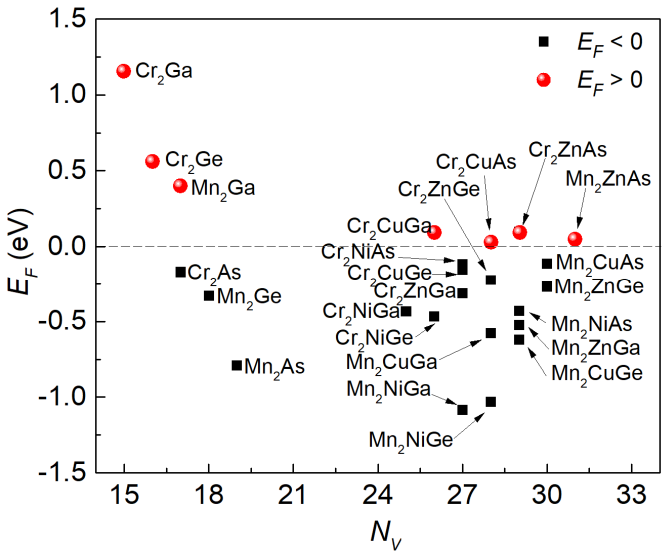

Figure 7. Formation energy vs N_V for Cr_2YZ and Mn_2YZ (Y = void, Ni, Cu, and Zn; Z = Ga, Ge, and As) alloys.

As observed in Mn_2Si, the symmetry of the crystal structure and the chemical environment of the magnetic ions significantly affect the magnetic properties. Table 2 shows the atomic and total magnetic moments of the selected alloys for both the XA-type and $L2_1$-type configurations. Note that XA-type Mn_2NiGa has been experimentally confirmed [45]. The calculated lattice constant a = 5.89 Å of the XA-type structure is very close to the experimental one a = 5.91 Å. The calculated M_t = 1.01 μ_B is less than the experimental one of 1.41 μ_B (measured at 5K) because Mn_2NiGa undergoes martensitic transformation at low temperatures. These results indicate the reliability of our calculations. The magnetic moments of Cr1 (M_{Cr1}) and Cr2 (M_{Cr2}) (or M_{Mn1} and M_{Mn2}) are antiparallelly aligned in the centrosymmetric $L2_1$-type configuration, and the magnitude of the magnetic moments is exactly the same, forming a typical AFM. The Y and Z atoms contribute no magnetic moment at all, and the M_t of the alloys is zero. Magnetic structure becomes more complex in the non-centrosymmetric XA-type structure. The M_{Cr1} and M_{Cr2} (or M_{Mn1} and M_{Mn2}) are still aligned in an antiparallel manner, but their magnitude is different. For example, in Mn_2Ge, M_{Mn1} and M_{Mn2} are close, while in Mn_2As, M_{Mn1} and M_{Mn2} differ greatly. The M_t of Mn_2Ge is also different from that of Mn_2As. The magnetism of the XA alloy is obviously closely related to the N_V.

Table 2. N_V, equilibrium lattice constants, atomic-resolved and total magnetic moments per unit cell in μ_B for Cr_2YZ and Mn_2YZ (Y = void, Ni, Cu, and Zn; Z = Ga, Ge, and As) full-Heusler alloys. Both the XA-type and $L2_1$ type structures were considered.

Alloys	N_V	Structure	a	M_{X1}	M_{X2}	M_Y	M_Z	M_t
Cr_2Ga	15	XA	5.92	4.11	−4.47	-	−0.09	−0.45
		$L2_1$	6.01	−4.76	4.76	-	0	0
Cr_2Ge	16	XA	5.82	3.67	−4.07	-	0.07	−0.46
		$L2_1$	5.90	−4.37	4.37	-	0	0
Cr_2As	17	XA	5.77	−3.77	3.57	-	0.03	−0.17
		$L2_1$	5.87	−4.31	4.31	-	0	0
Mn_2Ga	17	XA	5.76	−3.87	3.73	-	−0.05	−0.19
		$L2_1$	5.86	−4.38	4.38	-	0	0
Mn_2Ge	18	XA	5.63	−3.12	3.13	-	−0.01	0
		$L2_1$	5.84	−4.29	4.29	-	0	0

Table 2. *Cont.*

Alloys	N_V	Structure	a	M_{X1}	M_{X2}	M_Y	M_Z	M_t
Mn_2As	19	XA	5.64	−2.70	3.64	-	0.06	1.00
		$L2_1$	5.79	−3.98	3.98	-	0	0
Cr_2NiGa	25	XA	5.93	−3.63	4.05	0.35	0.05	0.83
		$L2_1$	6.03	−4.23	4.23	0	0	0
Cr_2NiGe	26	XA	5.85	−2.42	3.75	0.46	0.04	1.82
		$L2_1$	5.96	−3.79	3.79	0	0	0
Cr_2CuGa	26	XA	6.05	−4.08	4.35	0	0.03	0.30
		$L2_1$	6.10	−4.44	4.44	0	0	0
Cr_2NiAs	27	XA	5.89	−2.95	4.01	0.26	0.08	1.40
		$L2_1$	5.94	−3.51	3.51	0	0	0
Cr_2CuGe	27	XA	6.02	−3.93	4.20	−0.01	0.03	0.30
		$L2_1$	6.05	−4.20	4.20	0	0	0
Cr_2ZnGa	27	XA	6.13	−4.26	4.29	0	0.01	0.04
		$L2_1$	6.15	−4.48	4.48	0	0	0
Mn_2NiGa	27	XA	5.89	−3.32	4.05	0.21	0.07	1.01
		$L2_1$	5.93	−3.82	3.82	0	0	0
Cr_2CuAs	28	XA	6.08	−4.13	4.31	−0.01	0.04	0.21
		$L2_1$	6.08	−4.23	4.23	0	0	0
Cr_2ZnGe	28	XA	6.11	−4.06	4.17	0.03	0.01	0.15
		$L2_1$	6.16	−4.45	4.45	0	0	0
Mn_2CuGa	28	XA	5.93	−3.64	−3.96	−0.03	0.03	0.32
		$L2_1$	5.99	−3.99	3.99	0	0	0
Mn_2NiGe	28	XA	5.87	−3.20	3.93	0.06	0.08	0.88
		$L2_1$	5.87	−3.38	3.38	0	0	0
Mn_2NiAs	29	XA	5.90	−3.48	4.14	0.01	0.09	0.93
		$L2_1$	5.88	−3.25	3.25	0	0	0
Mn_2CuGe	29	XA	5.96	−3.47	4.02	−0.06	0.1	0.59
		$L2_1$	5.98	−3.76	3.76	0	0	0
Mn_2ZnGa	29	XA	6.05	−3.75	4.01	−0.06	0.09	0.29
		$L2_1$	6.08	−3.96	3.96	0	0	0
Cr_2ZnAs	29	XA	6.23	−4.27	4.48	0.05	0.01	0.28
		$L2_1$	6.25	−4.50	4.50	0	0	0
Mn_2CuAs	30	XA	5.98	−2.95	4.07	−0.04	0.13	1.21
		$L2_1$	6.00	−3.64	3.64	0	0	0
Mn_2ZnGe	30	XA	6.09	−3.57	4.02	−0.08	0.10	0.46
		$L2_1$	6.07	−3.70	3.70	0	0	0
Mn_2ZnAs	31	XA	6.12	−3.13	4.10	−0.11	0.14	1.01
		$L2_1$	6.08	−3.51	3.51	0	0	0

Figure 8 shows the N_V dependence of M_t for the selected Mn_2-based and Cr_2-based alloys. Among them, there are 9 $L2_1$-type alloys (red) and 11 XA-type alloys (black). It can be seen that the M_t of the alloys with an $L2_1$-type structure is exactly zero, and totally independent of N_V. This is because in a centrosymmetric $L2_1$-type structure, M_{Cr1} and M_{Cr2} (or M_{Mn1} and M_{Mn2}) are exactly the same magnitude and aligned in an antiparallel manner, so M_Y and M_Z have no contribution to M_t. However, the M_t and N_V of XA-type alloys have obvious correlation, following the Slater–Pauling rule. The deviation of M_t in some alloys from the Slater–Pauling curve is because they are not ideal half metals. For Mn_2Ge and Mn_2As, which are half metals, the M_t and N_V satisfy the rule of $M_t = N_V - 18$. Therefore, Mn_2YZ and Cr_2YZ (Y = void, Ni, Cu, and Zn; Z = Ga, Ge, and

As) alloys with $L2_1$-type structures are potential candidates for conventional AFM, while those with XA-type structures are promising candidates for compensated ferrimagnets.

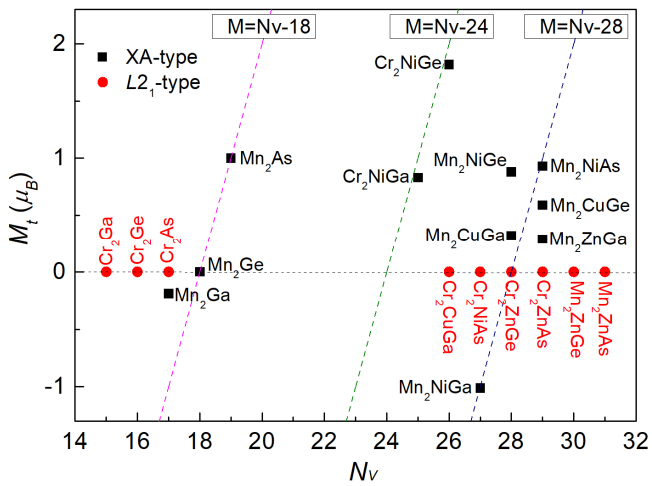

Figure 8. M_t vs N_V for Cr_2YZ and Mn_2YZ (Y = void, Ni, Cu, and Zn; Z = Ga, Ge, and As) full-Heusler alloys. The dotted lines represent the three typical Slater–Pauling curves.

Figure 9 shows the DOS of the alloys selected for study. Both the $L2_1$-type and XA-type structural configurations are provided for comparison. The DOS of alloys crystallized into $L2_1$-type configuration has no spin-polarized distribution, and the distributions of the DOS for the two spin directions are completely symmetric. The zero-spin polarization and zero net magnetic moment indicate all the nine alloys that crystallize into $L2_1$-type configurations are conventional AFMs. The DOS of alloys with XA-type configuration exhibit spin-polarized distribution. This is because in non-centrosymmetric XA-type Mn_2YZ and Cr_2YZalloys, Mn (or Cr) atoms at site A and B have different chemical environments, which results in an asymmetric distribution of DOS for the different Mn (or Cr) atoms and the DOS of these two Mn (or Cr) atoms cannot form a fully symmetric DOS without spin polarization. Therefore, the total DOS shows spin polarization, which is similar to $C1_b$-type Mn_2Si. Therefore, alloys with XA-type structural configurations have a chance to be HMFCF. However, not all selected alloys exhibit half-metallic and fully compensated ferrimagnetic properties. XA-type Cr_2NiGa has an energy gap in the spin-down channel, but is far away from the Fermi level. Only XA-type Cr_2NiGe, XA-type Mn_2CuGa, and XA-type Cr_2ZnGe have energy gaps near the Fermi level. Cr_2NiGe has an N_V of 26, so M_t is not zero but 1.82 μ_B, which is basically consistent with $M_t = N_V - 28$. The N_V of Cr_2ZnGe and Mn_2CuGa are both 28, so M_t is close to zero, and they can possibly form HMFCF. The HMFCF properties of XA-type Cr_2ZnGe have also been confirmed by other calculations.

Figure 10 shows the total energy differences between the tetragonal-distorted phase and cubic phase ($\Delta E = E_{tot}$ (c/a) $- E_{tot}$ (c/a = 1)) and total magnetic moment (M_t), as a function of c/a for alloys, including XA-type Cr_2NiGa, XA-type Mn_2CuGa, XA-type Mn_2CuGe, and $L2_1$-type Cr_2CuZ (Z = Ga, Ge and Sn). XA-type Cr_2NiGa has two energy minimums at c/a = 1 and c/a = 1.32 during the tetragonal distortion. The fact of ΔE (c/a = 1.32) < 0 indicates that the tetragonal phase is more stable than the cubic phase. XA-type Mn_2CuGa has no definite energy minimum in the range from 0.9 to 1.2 of c/a, indicating that the cubic phase and tetragonal phase may coexist in the same condition. XA-type Mn_2CuGe has a stable tetragonal phase (c/a = 1.16) and a metastable cubic phase (c/a = 1). $L2_1$-type Cr_2CuZ (Z = Ga, Ge and As) has an energy maximum at c/a = 1 and two energy minimums at c/a < 1 and c/a > 1. These results indicate that the cubic phase is an unstable state for $L2_1$-type Cr_2CuZ (Z = Ga, Ge and As), which is consistent with the positive E_F calculated for Cr_2CuGa and Cr2CuAs (Figure 7). The tetragonal distortion lowers the energy in the cubic phase and leads to a stable tetragonal phase, which has a negative E_F. The tetragonal phase that is distorted from the XA-type cubic phase is

non-centrosymmetric, resulting in the M_t of the alloys being very sensitive to the lattice distortion. The tetragonal phase that is distorted from the $L2_1$-type cubic phase is still centrosymmetric; thus, these alloys have very robust antiferromagnetic properties, with respect to the tetragonal distortion.

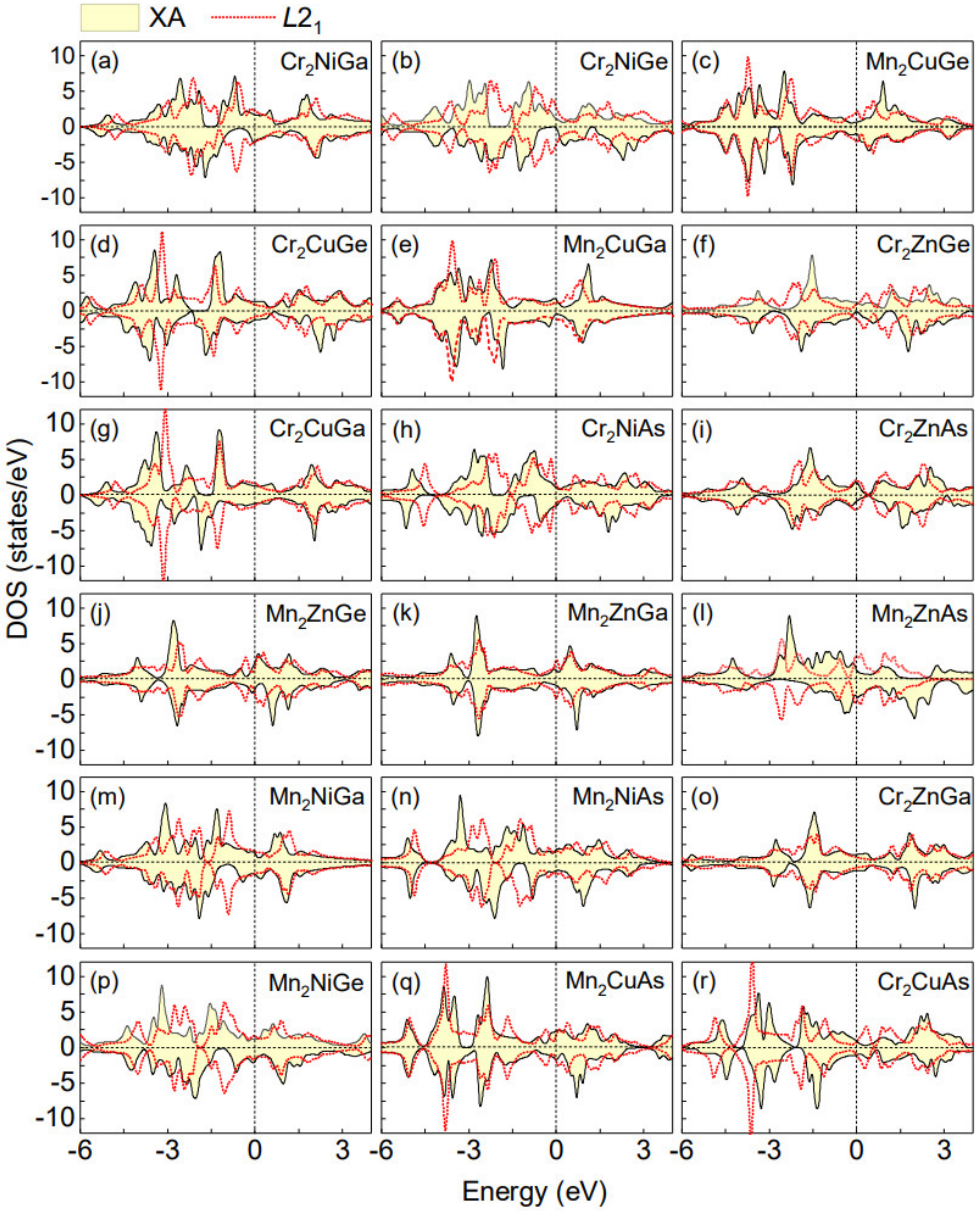

Figure 9. DOS per formula unit for both XA-type (yellow fill) and $L2_1$-type (red dotted line) structure configurations of (**a**) Cr_2NiGa, (**b**) Cr_2NiGe, (**c**) Mn_2CuGe, (**d**) Cr_2CuGe, (**e**) Mn_2CuGa, (**f**) Cr_2ZnGe, (**g**) Cr_2CuGa, (**h**) Cr_2NiAs, (**i**) Cr_2ZnAs, (**j**) Mn_2ZnGe, (**k**) Mn_2ZnGa, (**l**) Mn_2ZnAs, (**m**) Mn_2NiGa, (**n**) Mn_2NiAs, (**o**) Cr_2ZnGa, (**p**) Mn_2NiGe, (**q**) Mn_2CuAs and (**r**) Cr_2CuAs.

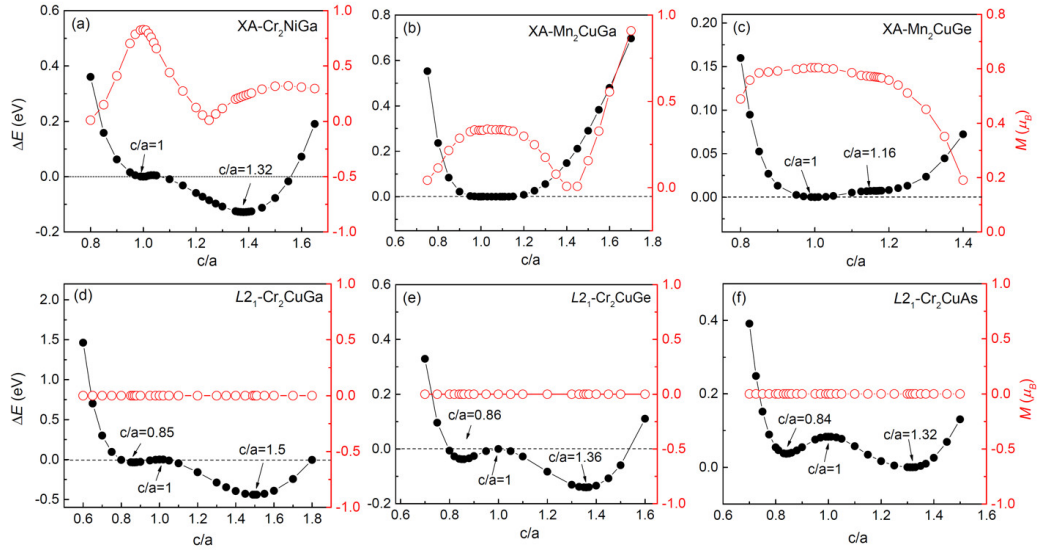

Figure 10. The total energy differences (black solid circle) between tetragonal-distorted phase and cubic phase ($\Delta E = E_{tot}$ (c/a) $- E_{tot}$ (c/a = 1)) and the corresponding magnetic moment (red hollow circle) as a function of c/a for (**a**) XA-type Cr_2NiGa, (**b**) XA-type Mn_2CuGa, (**c**) XA-type Mn_2CuGe, (**d**) $L2_1$-type Cr_2CuGa, (**e**) $L2_1$-type Cr_2CuGe, and (**f**) $L2_1$-type Cr_2CuAs alloys. The zero point corresponds to the energy in the cubic phase.

4. Conclusions

Due to the resulting zero net magnetic moment and high spin-polarization, HMFCFs are promising materials for future spintronic technology. In this paper, we discussed the phase stability, the site preference, the tetragonal distortion, and the influence of symmetry from the crystal structure and the chemical environments of magnetic ions on the magnetic properties of Mn_2YZ and Cr_2YZ (Y = void, Ni, Cu, and Zn; Z = Ga, Ge, and As) full-Heusler alloys. We found that the selected Cr_2-based alloys, except for Cr_2NiGa and Cr_2NiGe, prefer to crystallize into the centrosymmetric $L2_1$-type structure, while the selected Mn_2-based alloys, except for Mn_2CuAs, Mn_2ZnGe, and Mn_2ZnAs, tend to crystallize into the non-centrosymmetric XA-type structure. The distributions of the DOS in the selected alloys under study are strongly dependent on the symmetry of the crystal structure and the chemical environments of each Mn or Cr atom. Alloys with magnetic ions in different chemical environments can achieve (fully) compensated ferrimagnetism, even when the number of magnetic ions is even and less than three. The AFM state of Mn_2-based and Cr_2-based alloys with centrosymmetric structure is very stable and cannot be destroyed by changing N_V and tetragonal distortion, nor will spin-polarized DOS be generated. In contrast, the M_t of XA-type alloys with non-centrosymmetric structure depends heavily on N_V, tetragonal, and generated spin-polarized DOS. These results indicate that the magnetism, distribution of DOS, and spin polarizability of the non-centrosymmetric XA-type alloys selected in this study are highly tunable. Therefore, the selected alloys with $L2_1$-type structure and their tetragonal-distorted structure are potential candidates for conventional AFMs, while those with XA-type structure and their tetragonal-distorted structure are promising candidates for (fully) compensated ferrimagnets.

Author Contributions: Conceptualization, Y.Z.; Data curation, Z.W.; Supervision, Z.L. and X.M.; Writing—original draft, Z.W.; Writing—review and editing, Y.Z. and X.M. All authors have read and agreed to the published version of the manuscript.

Funding: This research was funded by the Science and Technology Plan Project of Guangzhou (No. 202102020934).

Data Availability Statement: Not applicable.

Conflicts of Interest: The authors declare no conflict of interest.

References

1. Šmejkal, L.; Mokrousov, Y.; Yan, B.; MacDonald, A.H. Topological antiferromagnetic spintronics. *Nat. Phys.* **2018**, *14*, 242. [CrossRef]
2. Marrows, C. Addressing an antiferromagnetic memory. *Science* **2016**, *351*, 558. [CrossRef] [PubMed]
3. Jungwirth, T.; Marti, X.; Wadley, P.; Wunderlich, J. Electrical switching of an antiferromagnet. *Nat. Nanotech.* **2016**, *11*, 231. [CrossRef] [PubMed]
4. Lebrun, R.; Ross, A.; Bender, S.A.; Qaiumzadeh, A.; Baldrati, L.; Cramer, J.; Brataas, A.; Duine, R.A.; Klaui, M. Tunable long-distance spin transport in a crystalline antiferromagnetic iron oxide. *Nature* **2018**, *561*, 222. [CrossRef]
5. Baltz, V.; Manchon, A.; Tsoi, M.; Moriyama, T.; Ono, T.; Tserkovnyak, Y. Antiferromagnetic spintronics. *Rev. Mod. Phys.* **2018**, *90*, 015005. [CrossRef]
6. Van Leuken, H.; de Groot, R. Half-Metallic Antiferromagnets. *Phys. Rev. Lett.* **1995**, *74*, 1171. [CrossRef]
7. Wurmehl, S.; Kandpal, H.C.; Fecher, G.H.; Felser, C. Valence electron rules for prediction of half-metallic compensated-ferrimagnetic behaviour of Heusler compounds with complete spin polarization. *J. Phys. Condens. Matter* **2006**, *18*, 6171. [CrossRef]
8. Akai, H.; Ogura, M. Half-Metallic Diluted Antiferromagnetic Semiconductors. *Phys. Rev. Lett.* **2006**, *97*, 026401. [CrossRef]
9. Hu, X. Half-Metallic Antiferromagnet as a Prospective Material for Spintronics. *Adv. Mater.* **2012**, *24*, 294. [CrossRef]
10. Manna, K.; Sun, Y.; Muechler, L.; Kübler, J.; Felser, C. Heusler, Weyl and Berry. *Nat. Rev. Mater.* **2018**, *3*, 244. [CrossRef]
11. Finley, J.; Lee, C.-H.; Huang, P.Y.; Liu, L. Cubic Mn_2Ga Thin Films: Crossing the Spin Gap with Ruthenium. *Adv. Mater.* **2018**, *31*, 1805361. [CrossRef] [PubMed]
12. Kurt, H.; Rode, K.; Stamenov, P.; Venkatesan, M.; Lau, Y.C.; Fonda, E.; Coey, J.M.D. Cubic Mn_2Ga Thin Films: Crossing the Spin Gap with Ruthenium. *Phys. Rev. Lett.* **2014**, *112*, 027201. [CrossRef] [PubMed]
13. Skaftouros, S.; Ozdogan, K.; Sasioglu, E.; Galanakis, I. Search for spin gapless semiconductors: The case of inverse Heusler compounds. *Appl. Phys. Lett.* **2013**, *102*, 022402. [CrossRef]
14. Jia, H.Y.; Dai, X.F.; Wang, L.Y.; Liu, R.; Wang, X.T.; Li, P.P.; Cui, Y.T.; Liu, G.D. Doping effect on electronic structures and band gap of inverse Heusler compound: Ti_2CrSn. *J. Magn. Magn. Mater.* **2014**, *367*, 33. [CrossRef]
15. Jia, H.Y.; Dai, X.F.; Wang, L.Y.; Liu, R.; Wang, X.T.; Li, P.P.; Cui, Y.T.; Liu, G.D. Ti_2MnZ (Z = Al, Ga, In) compounds: Nearly spin gapless semiconductors. *Advances* **2014**, *4*, 047113. [CrossRef]
16. Zhang, Y.J.; Liu, Z.H.; Liu, E.K.; Liu, G.D.; Ma, X.Q.; Wu, G.H. Towards fully compensated ferrimagnetic spin gapless semiconductors for spintronic applications. *Europhys. Lett.* **2015**, *111*, 37009. [CrossRef]
17. Fang, Q.-L.; Zhao, X.-M.; Zhang, J.-M.; Xu, K.-W. Magnetic properties and half-metallic in bulk and (001) surface of Ti_2MnAl Heusler alloy with Hg_2CuTi-type structure. *Thin Solid Film.* **2014**, *558*, 241. [CrossRef]
18. Zhang, Y.J.; Liu, Z.H.; Liu, G.D.; Ma, X.Q.; Cheng, Z.X. Robust fully-compensated ferrimagnetism and semiconductivity in inverse Heusler compounds: Ti_2VZ (Z = P, As, Sb, Bi). *J. Magn. Magn. Mater.* **2018**, *449*, 515. [CrossRef]
19. Galanakis, I.; Özdoğan, K.; Şaşıoğlu, E.; Aktaş, B. Ab initio design of half-metallic fully compensated ferrimagnets: The case of Cr_2MnZ (Z = P, As, Sb, and Bi). *Phys. Rev. B* **2007**, *75*, 172405. [CrossRef]
20. Galanakis, I. First-principles electronic and magnetic properties of the half-metallic antiferromagnet Cr2MnSb. *J. Magn. Magn. Mater.* **2009**, *321*, L34.
21. Galanakis, I.; Ozdogan, K.; Sasioglu, E.; Aktas, B. Doping of Mn_2VAl and Mn_2VSi Heusler alloys as a route to half-metallic antiferromagnetism. *Phys. Rev. B* **2007**, *75*, 092407. [CrossRef]
22. Manuel, M.M.; Geisler, P. Phase stability of chromium based compensated ferrimagnets with inverse Heusler structure. *J. Magn. Magn. Mater.* **2013**, *341*, 72.
23. Galanakis, I.; Şaşıoglu, E. High T_C half-metallic fully-compensated ferrimagnetic Heusler compounds. *Appl. Phys. Lett.* **2011**, *99*, 052509. [CrossRef]
24. Žic, M.; Rode, K.; Thiyagarajah, N.; Lau, Y.-C.; Betto, D.; Coey, J.M.D.; Sanvito, S.; O'Shea, K.J.; Ferguson, C.A.; MacLaren, D.A.; et al. Designing a fully compensated half-metallic ferrimagnet. *Phys. Rev. B* **2016**, *93*, 140202. [CrossRef]
25. Zhang, Y.J.; Liu, Z.H.; Liu, G.D.; Ma, X.Q. Half-metallic fully compensated ferrimagnetism in C1b-type half Heusler compounds $Mn_2Si_{1-x}Ge_x$. *J. Magn. Magn. Mater.* **2015**, *387*, 67. [CrossRef]
26. Luo, H.Z.; Liu, G.D.; Meng, F.B.; Wang, W.H.; Wu, G.H.; Zhu, X.X.; Jiang, C.B. Half-metallicity and magnetic properties of half-Heusler type Mn_2Sn: Ab initio predictions. *Phys. B* **2011**, *406*, 4245. [CrossRef]
27. Wang, X.; Cheng, Z.; Wang, J.; Liu, G. A full spectrum of spintronic properties demonstrated by a $C1_b$-type Heusler compound Mn 2 Sn subjected to strain engineering. *J. Mater. Chem. C* **2016**, *4*, 8535. [CrossRef]
28. Galanakis, I.; Özdoğan, K.; Şaşıoglu, E. High-T_C fully compensated ferrimagnetic semiconductors as spin-filter materials: The case of CrVXAl (X= Ti, Zr, Hf) Heusler compounds. *J. Phys. Condens. Matter* **2014**, *26*, 086003. [CrossRef]
29. Venkateswara, Y.; Gupta, S.; Samatham, S.S.; Varma, M.R.; Suresh, K.G.; Alam, A. Competing magnetic and spin-gapless semiconducting behavior in fully compensated ferrimagnetic CrVTiAl: Theory and experiment. *Phys. Rev. B* **2018**, *97*, 054407. [CrossRef]
30. Zhang, Y.J.; Liu, Z.H.; Wu, Z.G.; Ma, X.Q. Prediction of fully compensated ferromagnetic spin-gapless semiconducting FeMnGa/Al/In half Heusler alloys. *IUCrJ* **2019**, *6*, 610. [CrossRef]

31. Lamrani, A.F.; Ouchri, M.; Benyoussef, A.; Belaiche, M.; Loulidi, M. Half-metallic antiferromagnetic behavior of double perovskite Sr_2OsMoO_6: First principle calculations. *J. Magn. Magn. Mater.* **2013**, *345*, 195. [CrossRef]
32. Heusler, F.; Dtsch, V. Über magnetische manganlegierungen. *Phys. Ges.* **1903**, *5*, 219.
33. Graf, T.; Felser, C.; Parkin, S.S.P. Simple rules for the understanding of Heusler compounds. *Prog. Solid State Chem.* **2011**, *39*, 1. [CrossRef]
34. Galanakis, I.; Dederichs, P.; Papanikolaou, N. Origin and properties of the gap in the half-ferromagnetic Heusler alloys. *Phys. Rev. B* **2002**, *66*, 134428. [CrossRef]
35. Galanakis, I.; Dederichs, P.; Papanikolaou, N. Slater-Pauling behavior and origin of the half-metallicity of the full-Heusler alloys. *Phys. Rev. B* **2002**, *66*, 174429. [CrossRef]
36. Skaftouros, S.; Özdoğan, K.; Şaşıoğlu, E.; Galanakis, I. Generalized Slater-Pauling rule for the inverse Heusler compounds. *Phys. Rev. B* **2013**, *87*, 024420. [CrossRef]
37. Ozdogan, K.; Galanakis, I.; Sasioglu, E.; Atkas, B. Search for half-metallic ferrimagnetism in V-based Heusler alloys Mn_2VZ (Z = Al, Ga, In, Si, Ge, Sn). *J. Phys. Condens. Matter* **2006**, *18*, 2905. [CrossRef]
38. Yousuf, S.; Gupta, D.C. Robustness in spin polarization and thermoelectricity in newly tailored Mn_2-based Heusler alloys. *Indian J. Phys.* **2018**, *92*, 855. [CrossRef]
39. Nayak, A.K.; Kumar, V.; Ma, T.; Werner, P.; Pippel, E.; Sahoo, R.; Damay, F.; Rößler, U.K.; Felser, C.; Parkin, S.S.P. Magnetic antiskyrmions above room temperature in tetragonal Heusler materials. *Nature* **2017**, *548*, 561. [CrossRef]
40. Liu, Z.H.; Zhang, Y.J.; Zhang, H.G.; Zhang, X.J.; Ma, X.Q. Giant exchange bias in Mn_2FeGa with hexagonal structure. *Appl. Phys. Lett.* **2016**, *109*, 032408. [CrossRef]
41. Nayak, A.K.; Nicklas, M.; Chadov, S.; Khuntia, P.; Shekhar, C.; Kalache, A.; Baenitz, M.; Skourski, Y.; Guduru, V.K.; Puri, A.; et al. Design of compensated ferrimagnetic Heusler alloys for giant tunable exchange bias. *Nat. Mater.* **2015**, *14*, 679. [CrossRef] [PubMed]
42. Ouardi, S.; Fecher, G.H.; Felser, C. Realization of Spin Gapless Semiconductors: The Heusler Compound Mn_2CoAl. *Phys. Rev. Lett.* **2013**, *110*, 100401. [CrossRef] [PubMed]
43. Kreiner, G.; Kalache, A.; Hausdorf, S.; Alijani, V.; Qian, J.-F.; Shan, G.; Burkhardt, U.; Ouardi, S.; Felser, C. New Mn_2-based Heusler compounds. *Z. Anorg. Allg. Chem.* **2014**, *640*, 738. [CrossRef]
44. Faleev, S.V.; Ferrante, Y.; Jeong, J.; Samant, M.G.; Jones, B.; Parkin, S.S.P. Origin of the tetragonal ground state of Heusler compounds. *Phys. Rev. Appl.* **2017**, *7*, 034022. [CrossRef]
45. Liu, G.D.; Chen, J.L.; Liu, Z.H.; Dai, X.F.; Wu, G.H.; Zhang, B.; Zhang, X.X. Martensitic transformation and shape memory effect in a ferromagnetic shape memory alloy: Mn_2NiGa. *Appl. Phys. Lett.* **2005**, *87*, 262504. [CrossRef]
46. Hafner, J. Ab-initio simulations of materials using VASP: Density-functional theory and beyond. *J. Comput. Chem.* **2008**, *29*, 2044. [CrossRef]
47. Perdew, J.P. Density-functional approximation for the correlation energy of the inhomogeneous electron gas. *Phys. Rev. B* **1986**, *33*, 8822. [CrossRef]
48. Perdew, J.P.; Yue, W. Accurate and simple density functional for the electronic exchange energy: Generalized gradient approximation. *Phys. Rev. B* **1986**, *33*, 8800. [CrossRef]
49. Mavropoulos, P.; Galanakis, I.; Popescu, V.; Dederichs, P.H. The influence of spin–orbit coupling on the band gap of Heusler alloys. *J. Phys. Condens. Matter* **2004**, *16*, S5759. [CrossRef]
50. Blaha, P.; Schwarz, K.; Madsen, G.K.; Kvasnicka, D.; Luitz, J. *WIEN2K: An Augmented Plane Wave Plus Local Orbitals Program for Calculating Crystal Properties*; Vienna University of Technology: Vienna, Austria, 2001.
51. Wang, X.L. Proposal for a new class of materials: Spin gapless semiconductors. *Phys. Rev. Lett.* **2008**, *100*, 156404. [CrossRef]
52. Fujii, S.; Ishida, S.; Asano, S. High Spin Polarization of Ferrimagnetic Half-Heusler Compounds FeCrZ and MnYZ (Y = Mn, Cr; Z = IIIb, IVb, Vb Elements). *J. Phys. Soc. Jpn.* **2010**, *79*, 124702. [CrossRef]
53. Balke, B.; Fecher, G.H.; Winterlik, J.; Felser, C. Mn_3Ga, a compensated ferrimagnet with high Curie temperature and low magnetic moment for spin torque transfer applications. *Appl. Phys. Lett.* **2007**, *90*, 152504. [CrossRef]
54. Ma, J.; He, J.; Mazumdar, D.; Munira, K.; Keshavarz, S.; Lovorn, T.; Ghosh, A.W.; William, H.B. Computational investigation of inverse Heusler compounds for spintronics applications. *Phys. Rev. B* **2018**, *98*, 094410. [CrossRef]
55. Guo, G.Y.; Botton, G.A.; Nishino, Y. Electronic structure of possible 3d 'heavy-fermion' compound. *J. Phys. Condens. Matter* **1998**, *10*, L119. [CrossRef]
56. Zhang, Y.J.; Liu, Z.H.; Liu, G.D.; Ma, X.Q. Structural, electronic and magnetic properties of $CoFeTiGa_{1-x}Sb_x$ compounds. *J. Magn. Magn. Mater.* **2017**, *422*, 32. [CrossRef]
57. Tan, J.G.; Liu, Z.H.; Zhang, Y.J.; Li, G.T.; Zhang, H.G.; Liu, G.D.; Ma, X.Q. Site preference and tetragonal distortion of Heusler alloy Mn-Ni-V. *Results Phys.* **2009**, *321*, L34. [CrossRef]
58. Liu, G.; Dai, X.; Liu, H.; Chen, J.; Li, Y.; Xiao, G.; Wu, G. Mn_2CoZ (Z = Al, Ga, In, Si, Ge, Sn, Sb) compounds: Structural, electronic, and magnetic properties. *Phys. Rev. B* **2008**, *77*, 014424. [CrossRef]
59. Zhang, Y.J.; Li, G.J.; Liu, E.K.; Chen, J.L.; Wang, W.H.; Wu, G.H. Ferromagnetic structures in Mn_2CoGa and Mn_2CoAl doped by Co, Cu, V, and Ti. *J. Appl. Phys.* **2013**, *113*, 123901.
60. Geiersbach, U.; Bergmann, A.; Westerholt, K. Structural, magnetic and magnetotransport properties of thin films of the Heusler alloys Cu_2MnAl, Co_2MnSi, Co_2MnGe and Co_2MnSn. *J. Magn. Magn. Mater.* **2002**, *240*, 546. [CrossRef]

61. Amari, S.; Dahmane, F.; Omran, S.B.; Doumi, B. Theoretical investigation of the structural, magnetic and band structure characteristics of $Co_2FeGe_{1-x}Si_x$ (x = 0, 0.5, 1) full-Heusler alloys. *J. Korean Phys. Soc.* **2016**, *69*, 1462. [CrossRef]
62. Wang, X.; Cheng, Z.; Yuan, H.; Khenata, R. $L2_1$ and XA ordering competition in titanium-based full-Heusler alloys. *J. Mater. Chem. C* **2017**, *5*, 11559. [CrossRef]
63. Du, X.; Zhang, Y.; Liu, Z.; Wu, Z.; Xu, S.; Ma, X. Site preference, magnetic and electronic properties of half-metallic Vanadium-based full Heusler alloys. *J. Magn. Magn. Mater.* **2021**, *517*, 167379. [CrossRef]
64. Berri, S. Electronic structure and half-metallicity of the new Heusler alloys PtZrTiAl, PdZrTiAl and $Pt_{0.5}Pd_{0.5}ZrTiAl$. *Chin. J. Phys.* **2017**, *55*, 195. [CrossRef]
65. Paudel, R.; Zhu, J.C. Investigation of half-metallicity and magnetism of bulk and (111)-surfaces of Fe_2MnP full Heusler alloy. *Vacuum* **2019**, *164*, 336. [CrossRef]
66. Paudel, R.; Kaphle, G.C.; Batouche, M.; Zhu, J.C. Half-metallicity, magnetism, mechanical, thermal, and phonon properties of FeCrTe and FeCrSe half-Heusler alloys under pressure. *Int. J. Quantum Chem.* **2020**, *120*, e26417. [CrossRef]